SAND2000-1228J
Submission to J. of Adhesion

Use of Self-Assembled Monolayers at Variable Coverage to Control Interface Bonding in a Model Study of Interfacial Fracture: Pure Shear Loading

M.S. Kent, H. Yim, A. Matheson, C. Cogdill, G. Nelson, E. D. Reedy
Sandia National Laboratories, Albuquerque, NM.

ABSTRACT

The relationships between fundamental interfacial interactions, energy dissipation mechanisms, and fracture stress or fracture toughness in a glassy thermoset / inorganic solid joint are not well understood. This subject is addressed with a model system involving an epoxy adhesive on a polished silicon wafer containing its native oxide. The proportions of physical and chemical interactions at the interface, and the in-plane distribution, are varied using self-assembling monolayers of octadecyltrichlorosilane (ODTS). The epoxy interacts strongly with the bare silicon oxide surface, but forms only a very weak interface with the methylated tails of the ODTS monolayer. The fracture stress is examined as a function of ODTS coverage in the napkin-ring (pure shear) loading geometry. The relationship between fracture stress and ODTS coverage is catastrophic, with a large change in fracture stress occurring over a narrow range of ODTS coverage. This transition in fracture stress does not correspond to a wetting transition of the epoxy. Rather, the transition in fracture stress corresponds to the onset of deformation in the epoxy, or the transition from brittle to ductile fracture. We postulate that the transition in fracture stress occurs when the local stress that the interface can support becomes comparable to the yield stress of the epoxy. The fracture results are independent of whether the ODTS deposition occurs by island growth (T_{dep}= 10 °C) or by homogeneous growth (T_{dep} = 24 °C).

Sandia is a multiprogram laboratory operated by Sandia Corporation, a Lockheed Martin Company, for the United States Department of Energy under contract DE-AC04-94AL85000.

DISCLAIMER

I. INTRODUCTION

Much effort in adhesion science has been devoted toward understanding the relationship between fundamental interfacial interactions and engineering fracture quantities such as joint strength or fracture energy [1-14]. These relationships are important from the standpoint of designing interfacial chemistry sufficient to provide the level of mechanical strength required for a particular application. In addition, such relationships are also important for understanding the effects of surface contamination. Different types of contamination, or different levels of contamination, likely impact joint strength and fracture toughness in different ways. Furthermore, the relationship is also important from the standpoint of aging. If interfacial chemical bonds scission over time due to the presence of a contaminant such as water, or exposure to UV or other radiation, etc, the relationships between joint strength or fracture energy and interface strength are important for lifetime prediction. A fundamental understanding of the relationship between the nature and spatial distribution of interfacial interactions and joint strength and fracture energy will give insight into these important issues.

The relationships between fundamental interfacial interactions and joint strength or fracture energy clearly depend upon both the mechanical properties of the adhesive and the nature of the interfacial interactions. For a perfectly brittle fracture, joint strength and fracture energy are proportional to the interface strength. However, dissipation occurs in real systems and the relationship between interface strength and the amount of energy dissipated during fracture depends upon the dissipation mechanism.

For certain cases, characterization of the interface in terms of the component surface energies and the interfacial energy appears to be sufficient. Mittal has reviewed previous work involving glassy thermosetting adhesives on low surface energy substrates such as polyethylene and polytetrafluoroethylene, where the interactions are of a physical nature [7]. In this case, the interactions are reversible, and no change in the fracture

mechanism occurs over the range of interface strength examined. Much data supports a correlation between fracture stress and thermodynamic work of adhesion ($W_a = \gamma_{air/adhes.} + \gamma_{air/substr.} - \gamma_{adhes./substr.}$ where $\gamma_{i/j}$ are interfacial energies), typically determined from contact angle and surface tension measurements using the uncured adhesive. Another well-studied case is that of elastomers in contact with inorganic substrates. Here, the fracture energy has been shown to be separable into a product of the intrinsic interface energy and a dissipation function which depends upon rate and temperature. [8-10] If the elastomer interacts with the substrate through only van der Waals interactions, the intrinsic interface energy approaches W_a at low rates. However, if the elastomer is covalently bonded to the substrate, the interactions are not reversible and the intrinsic interface energy is not related to W_a. For either case, the viscoelastic material response which determines the amount of energy dissipated is governed by monomeric friction and described by time-temperature superposition using the WLF equation. An energy description of the interface is again sufficient because the fracture mechanism remains the same at all interface strength or local stress levels.

On the other hand, for certain adhesive/adherend combinations the fracture mechanisms change as a function of interface strength. In this case an understanding of local stress is required, since changes in fracture mechanisms are triggered at particular local stress levels. One such example is interfacial fracture involving glassy thermoplastic polymers. Fracture between thermoplastic polymers has been studied as a function of the presence of block copolymers at the interface which form cross-ties between the two polymers [11-13]. In these systems the fracture mechanisms include chain pull-out, chain scission, and crazing. Transitions between these mechanisms have been determined based on the local stress required for bond scission or crazing, and the maximum stresses that the interface can support (dependent upon the molecular weight and areal density of block copolymer chains).

In the present work we consider glassy thermoset adhesives cured onto high surface energy substrates where strong chemical interactions can occur. In this case, plastic deformation within the adhesive is the major contribution to energy dissipation. For plastic deformation to occur in glassy thermoset polymers, a minimum local stress level (σ_y) must be attained. For a sufficiently weak interface, σ_y is not attained prior to interfacial separation, and little energy is dissipated within the adhesive. On the other hand, for a sufficiently strong interface, local stresses exceed σ_y and much plastic deformation and energy dissipation occur. We argue below that this determines a transition in fracture stress for the present system as a function of the interface strength. Since the onset of the nonlinear material response is triggered at a particular local stress level, the analysis must involve a characterization of the interface in terms of strength or local stress rather than energy. We focus on the extent of interfacial bonding needed to attain σ_y locally, and the relationship between the onset of deformation and the transition from adhesive-to-cohesive failure in pure shear loading.

When a crack is present on an interface, the general criteria for propagation are well understood. For an interfacial crack to propagate, the strain energy released must equal the energy required to separate the materials, or the fracture toughness [4]. It is also true that for a crack to propagate, the stress at the crack tip must reach values sufficient to cleave the interfacial interactions. The magnitude of the local stress that the interface can support, and the mode mixity, determine the degree of plastic deformation (plastic zone size and shape) and the fracture toughness. However, when a joint without a macroscopic crack in the bond-line is loaded, the factors which control stress concentration are less clear. In this work, the napkin-ring (NR) pure shear torsion test was used, which corresponds to the latter situation. Thus, a general understanding of the fracture behavior is discussed in terms of local stresses, but a quantitative analysis of stress profiles within the bond line has not yet been carried out. Nor have the sources of

stress concentration been uniquely identified. A corresponding study involving a nearly mode I fracture toughness test will be reported in a future publication.

The present model system involves an epoxy adhesive on a polished silicon wafer containing its native oxide. The interfacial interactions are varied systematically over a wide range using self-assembling monolayers (SAMs) of octadecyltrichlorosilane (ODTS). The epoxy interacts strongly with the bare silicon oxide surface through acid-base interactions involving the acidic silanol groups on the silicon oxide surface and the basic amine groups of the crosslinker [15]. However, the epoxy interacts through only very weak van der Waals interactions with the methylated tails of the ODTS chains. We examined the fracture behavior of such joints as a function of the ODTS coverage, thereby systematically varying the proportions of acid-base and van der Waals interfacial interactions. The polished silicon substrates provide very smooth surfaces, which allowed for a pure shear loading down to very small length scales. (Roughness on the substrate surface would introduce a tensile component to the local stress field near the surface.) The smooth surfaces also allowed extensive characterization of the SAM prior to applying the epoxy and also after fracture. SAM chemistry using trichlorosilane end groups on silicon oxide is well established [16-19]. By varying the deposition temperature, the deposition can occur by either island growth or single chain growth. Both cases were examined in this work.

II. EXPERIMENTAL

Materials. The substrates used in this study were polished single crystal silicon wafers (type P, orientation 100) from SilicaTek and Monsanto. The substrate thickness was 600-650 μm. This thickness is larger than the standard thickness of silicon wafers, and was necessary to avoid fracture of the silicon. ODTS was obtained from Akros. Anhydrous hexadecane and anhydrous carbon tetrachloride were obtained from Aldrich. Research grade EPON 828 resin was obtained from Shell. The crosslinker Jeffamine T-403 was

obtained from Huntsman Chemical Co. All materials were stored in a N_2-purged dry box and used as received. Deuterated epoxy resin was synthesized using deuterated bisphenol A and epichlorohydrin. The synthesis and purification procedures have been described in detail elsewhere [20].

Methods. The wafers were cleaned in a UV-ozone chamber and then submerged in a hexadecane/carbon tetrachloride solution containing ODTS. The coverage of ODTS was varied by controlling the time of exposure to the solution. The SAM-coated wafers were sonicated in toluene to remove nonbonded material, and then were blown dry with a stream of dry nitrogen.

All contact angle measurements were made with an Advanced Surface Technology, Inc. VCA 2500 Video Contact Angle System. Advancing (receding) contact angles were measured by slowly adding (removing) liquid from the drop with a syringe and recording the maximum (minimum) contact angle. For the measurement of epoxy contact angles, it was necessary to coat the tip of the syringe needle with a fluorinated material so that the epoxy did not wet the needle. A 3% solution of Teflon AF-1600 (Dupont) in Fluorinert (3M) was used to coat the needle. The coating was cured at 108°C for a minimum of 40 minutes.

The mass coverage of ODTS was determined by X-ray reflectivity using a Scintag X_1 powder diffractometer equipped with Cu Kα radiation, an incident beam mirror, and a Peltier-cooled solid-state Ge detector. The incident beam mirror was used to generate a parallel beam (in the height dimension) from the divergent x-ray source. A variable slit system at the exit port of the mirror housing was dialed to create a beam of 50 microns in height; the beam width in the non-parallel direction was 10mm. The technique and data analysis methods have been reviewed elsewhere [21].

The majority of the fracture tests were performed with steel rings having an I.D. of 20.98 mm and an O.D. of 23.19 mm (±0.03 mm). One set of tests was performed using rings with an I.D. of 10.43 mm and an O.D. of 12.21 mm. To remove machine oil, the rings were sonicated in an acetone bath for 30 min. The rings were then sandblasted to roughen the surface, soaked in isopropyl alcohol, and then air dried. After cleaning, the sandblasted rings were coated with aminopropyltriethoxysilane (Aldrich)) coupling agent solution: 250 ml distilled water, 0.20 ml formic acid 94%, and 1.25 ml aminopropyltriethoxysilane. The solution was stirred for 10 minutes prior to application. The rings were dipped into the solution and then heated for one hour at 90°C.

The two epoxy components were combined at a ratio of 46 parts by weight T403 per 100 parts resin and mixed by hand for 5 minutes using a metal spatula. The mixture was then placed in an oven at 60°C for 10 minutes to release air bubbles caused from mixing. The epoxy was applied to the rings, and the rings were then placed onto the ODTS-treated silicon substrates. The bond thickness, measured with a Dektak profilometer, was in the range of 50-60 μm. The ring/wafer sets were then heated in an oven at 50°C for 2 days to cure the epoxy. This low temperature cure was used to minimize residual thermal stresses.

The samples were fractured in the napkin-ring pure shear torsion geometry using a Mitutoyo Datatorq digital torque wrench mounted in a home-made goniometer. In these experiments the rate was not precisely controlled, but was roughly 60 deg/min. The applied shear stress at fracture (σ) is obtained from the maximum torque value (T) using the relation [22]

$$\sigma = T/(2\pi r^2 h) \qquad (1)$$

where r is the radius of the ring and h is the wall thickness. We assume that the napkin-ring test measures the critical local shear stress required for a crack to initiate. Once this critical stress state is reached, the crack propagates in an unstable manner. We were unable to locate the initiation site.

AFM images were obtained using a Park Scientific Autoprobe LF in either noncontact or lateral force tapping mode. SEM images were obtained using a JEOL JSM 6400XV electron microscope. Optical micrographs were obtained using a Leitz Orthoplan optical microscope (50x to 500x magnification) using interference contrast reflected light illumination. A thin coating of gold was applied to the surfaces of the fractured rings in order to avoid imaging the underlying roughened steel.

III. RESULTS

III.1 Characterization of ODTS layers

Several techniques have been used to characterize the ODTS monolayers prior to applying the epoxy: atomic force microscopy, advancing and receding contact angles with both water and uncured epoxy, and X-ray reflectivity. Our goals were to determine the fractional mass coverage and the degree of in-plane heterogeneity. These features are clearly related to the distribution and proportion of fundamental interactions between the epoxy and the silicon oxide.

A. Atomic Force Microscopy. AFM was used to examine the degree of lateral heterogeneity within the incomplete monolayers. Previous reports have indicated island formation under certain conditions of temperature and chain length due to a lateral phase transition [17-19]. We prepared substrates with ODTS deposited both by island growth and homogeneous growth to determine whether this difference has any effect on the

fracture behavior. To accomplish this, ODTS layers were deposited at room temperature (~ 24 °C) from a hexadecane/carbon tetrachloride solution (4/1 by vol) containing 0.058 vol % ODTS, and also at 10 °C from a hexadecane/carbon tetrachloride solution (2.3/1 by vol) containing 0.050 vol % ODTS. AFM images in Figures 1a and 1b are representative of samples prepared at 24 °C and 10 °C, respectively. Island formation was apparent for depositions at 10 °C, but was entirely absent for depositions at room temperature. For depositions at 10 °C, the islands appeared to saturate the surface at an equilibrium water contact angle in the range of 107°-110°, and the surfaces appeared homogeneous for equilibrium water contact angles in the range of 110° -115°.

B. Contact angles. The ODTS coverage was varied by controlling the time the substrates were exposed to the treating solution. Figure 2 shows ODTS coverage, as indicated indirectly by the equilibrium water contact angle, as a function of the exposure time of the silicon wafer substrates in the room temperature ODTS solution. The form of this curve remained constant throughout our study, but the numerical values varied slightly from day to day. The variation is likely due to variable amounts of water on the wafer surfaces or in the solutions. To obtain multiple samples having the same coverage for the fracture study, trays containing at least ten wafer pieces were immersed into the treating solution and removed at the desired times. The equilibrium water contact angle was measured on each piece. The mean and standard deviation of the equilibrium water contact angle for the ten samples are reported along with the fracture stresses in the following section.

In Figure 3a and 3b advancing and receding water contact angles are reported as a function of the equilibrium water contact angle for depositions at room temperature and 10 °C, respectively. We focus on the regime of relatively high contact angles, or ODTS coverage, where a strong variation in the fracture behavior occurs. Whereas the AFM images in Figure 1 show a dramatic difference in the in-plane distribution of ODTS for

depositions at room temperature and 10 °C, very little difference in observed in the advancing and receding water contact angles. A slight difference occurs in the behavior of Δ, the difference between advancing and receding contact angle. For depositions at room temperature, Δ varies from roughly 15° at full coverage to 31° at the lower end of the range examined. Most of the variation in Δ occurs over the narrow range of equilibrium contact angle from ~103° to ~95°. For depositions at 10 °C, Δ varies from roughly 5° at full coverage (equilibrium contact angle of 115°) to 9° at an equilibrium contact angle of 107°, and reaches 29° at an equilibrium contact angle of 82°. The increase in Δ with decreasing ODTS coverage seen in both cases can indicate an increase in the degree of heterogeneity or roughness, or alternatively a hysteresis in the interaction of water with the monoloayer or substrate surface. We suspect the latter in this case since the contact angle data are nearly the same for the two different in-plane distributions of ODTS. We suspect that with decreasing ODTS coverage, water is able to access the head groups of the ODTS or the substrate surface and adsorb strongly.

Advancing and receding contact angles using the uncured resin–crosslinker mixture as a function of ODTS coverage (room temperature deposition) are shown in Figure 4, where again the ODTS coverage is reflected in the equilibrium water contact angle. Data were obtained only for the range of relatively high ODTS coverage. A finite contact angle is observed over the entire range of ODTS coverage examined. On the other hand, apparent complete wetting (contact angle ≤ 5°) was observed for the epoxy mixture on the native oxide of silicon in the absence of ODTS. In contrast to the results obtained with water, no variation in the difference between the advancing and receding contact angles was detected with the liquid epoxy. These results indicate that epoxy access to surface sites varies smoothly over this range of ODTS coverage, and also that no wetting transition occurs.

The fractional surface areas of silicon oxide and methyl groups that are presented to the epoxy at various ODTS coverages can be estimated using the contact angle data in Figures 3 and 4 and the Cassie relation [23]:

$$\cos \theta_L = x_1 \cos \theta_{L1} + (1-x_1) \cos \theta_{L2} \qquad (2)$$

where θ_L is the contact angle for a probe liquid L on the mixed surface, θ_{L1} and θ_{L2} are the contact angles of L on the pure component surfaces, and x_1 is the area fraction of component 1. This relation assumes that the surface tension of a heterogeneous surface is given by the surface area-weighted average of the surface tensions of the pure components. In Figure 5 the area fraction of methyl groups determined from eq. (2) is plotted versus equilibrium contact angle, where both the water and epoxy contact angle data were used. The relations are the same over the range of ODTS coverage where the strong variation in fracture stress occurs. This relationship can be used to estimate the relative proportions of physical and chemical interactions across the interface.

C. X-ray reflectivity. For depositions at 24 °C and 10 °C, the mass coverage of ODTS was determined by X-ray reflectivity over the range of coverage most relevant to the fracture study. Representative X-ray reflectivity data are shown in Figure 5 for depositions at 24 °C. The mass coverage obtained from integrating the fitted electron density profiles is shown in Figure 7 for a range of coverage corresponding to equilibrium contact angles from 95° to 115° (full coverage) for both deposition temperatures. Full coverage corresponds to a surface density of 1.9 mg/m^2 or 1 molecule/24.6 Å^2. This is a slightly lower density than reported by Wasserman et al. [16]. The relationship between advancing water contact angle and fractional coverage is

in good agreement with a previous study of Allara, et al, where coverage was determined by ellipsometry [24]. We note that the fractional mass coverage data in Figure 7 differ significantly from the area fractions determined from the Cassie equation in Figure 5. For example, at an equilibrium contact angle of 100°, the ODTS mass fraction is 0.65 but the area fraction of methyl groups determined from the Cassie relation is 0.87. This comparison suggests that the ODTS chains somehow restrict access to the surface beyond simply the number of sites which are chemically bonded.

The thickness of the ODTS layer is shown in Figure 8 for the two deposition temperatures. This plot shows a nearly constant thickness for depositions at 10 °C (island growth), indicating that the islands are close packed with the chains standing nearly vertical. On the other hand, the thickness increases with coverage for depositions at room temperature, indicating that the chains are tilted at lower coverage and then stand up as the chains become crowded on the surface.

III.2. Fracture stress using napkin-ring torsion test

In order to establish that the napkin-ring test measures a critical stress state, the ring diameter was varied by roughly a factor of 2. Load to failure was determined for rings bonded to bare silicon wafers (no ODTS). The data shown in Figure 9 indeed demonstrate that fracture occurs at a constant stress level independent of ring diameter according to eq. 1.

Fracture stress as a function of ODTS coverage is plotted in Figure 10a, where the latter is reflected in the equilibrium water contact angle. We note that for the case of full ODTS coverage, the joint did not fracture, but rather the ring could be rotated on the substrate indefinitely, requiring a substantial normal force to detach it from the surface. At this coverage, the test measures friction rather than a fracture stress. The shear stress

required to rotate the ring was below the detection limit of our torque wrench ($\leq$ 3 MPa). This is consistent with the values reported for shearing CH_3-terminated SAMs using the surface forces apparatus [25,26], which fall in the range 1-4 MPa, increasing with normal force. In Figure 10a a sharp transition in fracture stress is observed which occurs over a range of ODTS coverage corresponding to water contact angles in the range of 98° - 105°. The abscissa in Figure 10a can be converted to the fraction of methyl groups using the Cassie relation in Figure 5 or the fractional ODTS mass coverage from the X-ray reflectivity data in Figure 7. The fracture stress data are replotted in Figure 10b and 10c using these two methods. The nature of the fracture curve is the same in each case, however the transition in fracture stress appears at higher area fraction using the Cassie relation.

In Figure 10d we present the data in a fourth representation, where the abscissa is converted to γ_{lv} (1 + cos θ) based on the epoxy advancing contact angle data of Figure 4, where γ_{lv} is the surface tension of the epoxy and θ is the contact angle of the uncured epoxy on the substrate. The surface tension of the uncured epoxy was determined to be 34.3 mJ/m^2 by the Wilhelmy plate technique. The value of the abscissa ranges from 52.5 to 68.6 mJ/m^2. The quantity γ_{lv} (1 + cos θ) is usually equated with W_a [1,2,23]. However, in this case γ_{lv} (1 + cos θ) represents only the work required to separate the uncured epoxy from the substrate, and does not account for chemical bonds formed during cure. The work to separate chemically bonded surfaces is of order 1 J/m^2 or greater [1], far above that calculated from the Young-Dupre equation. We argue below that representation of the interface in terms of the interfacial energies is not useful for understanding the transition in fracture stress. We note that much data in the literature for thermosetting adhesives on low surface energy solids (such as polytetrafluoroethylene and polyethylene) shows a linear relationship between fracture strength and $W_a = \gamma_{lv}$ (1 +

cos θ) [7], which contrasts sharply with the present data for epoxy on silicon. This important difference is due to the presence of chemical bonds in the present case, whereas only physical interactions occur in the former cases. We argue below that the presence of stronger interactions leads to a transition in the mode of fracture from brittle to ductile for pure shear loading. Another important difference is that some of the previous work involved tensile loading. The mode of loading is critically important in that nonlocal van der Waals interactions do not contribute to the fracture stress in pure shear, but make a large contribution for tensile loading.

Figures 10a-10c also include fracture data for samples in which ODTS was deposited at 10 °C, where island formation is observed by AFM. The fracture behavior is indistinguishable from that for depositions at room temperature. We also note that the fracture behavior was unchanged from that in Figure 10 following extensive filtration to remove dust particles.

III.3 Characterization of fracture surfaces

Visual examination of the fracture surfaces suggests a complete absence of epoxy on the substrates for ODTS coverages corresponding to equilibrium water contact angles from 115° to roughly 98°. Furthermore, no epoxy could be detected on the substrate by AFM, SEM, or optical microscopy over this range as well. In order to test more rigorously for the presence of epoxy on the substrate after fracture, additional samples were prepared with a deuterated epoxy resin and TOF-SIMS analysis was performed following fracture. Deuterium labeling allowed the presence of the epoxy resin to be distinguished from adventitious hydrocarbon material. Calibration was performed using a ~30 Å film of deuterated epoxy. [27] The data are shown in Figure 11, expressed as the ratio of the intensity of D^- ions to Si ions, and divided by the integrated signal resulting

from the 30 Å d-epoxy film. While the level of deuterium on the substrate is significantly above the background and increases noticeably over the range of ODTS coverage where the fracture stress rises, even the highest level of deuterium detected is far below that for the 30 Å d-epoxy film. In fact, the quantity of deuterium observed corresponds to only a very small fraction of a monolayer of deuterated epoxy. Several areas on the substrate surfaces were examined with the same result. This is strong evidence that the fracture remains truly interfacial in this range of ODTS coverage.

Examination of the surfaces of the rings by optical microscopy revealed the extent of deformation of the epoxy. No deformation was detected for the range of water contact angle from 115° - 104°, but rather the epoxy surface retained the smooth character of the polished silicon substrate. On the other hand, substantial deformation was observed for the range 103° - 98°, with the amount of deformation increasing with decreasing water contact angle. Representative images are shown in Figures 12a-12c. This deformation is the only significant observation coincident with the strong increase in the fracture stress. The length scale of the deformation is macroscopic, and the deformation patterns do not appear to be derived from the propagation of the crack.

For ODTS coverages corresponding to water contact angles less than 98°, macroscopic quantities of epoxy were observed visually on the substrates. Near 98°, typically only one small spot of epoxy remained on the substrate surface. With decreasing ODTS coverage, the area fraction covered by epoxy after fracture increased. For bare silicon wafers (no ODTS), epoxy was observed on the substrate over nearly the entire surface which was in contact with the ring.

IV. DISCUSSION

Through the use of self-assembling ODTS monolayers, we have explored the relationship between the strength of interfacial interactions and the fracture stress for pure shear loading. From Figure 10 it is clear that this relationship is highly nonlinear and catastrophic. The sharp breaks in the slope of the curve suggest changes in the fracture mechanism. Our goal is to understand the changes in fracture mechanism and the criterion that determines the transition in fracture stress. Below we discuss the observations and fracture mechanisms in terms of three regimes of ODTS coverage as indicated by equilibrium water contact angle: 115° - 104 ° (regime I), 104°- 98 ° (regime II), and 98° - 0° (regime III).

Regime I. Adhesive/brittle. In regime I, the failure is purely interfacial. In addition, no deformation of the epoxy is detectable by AFM, SEM, or optical microscopy. We postulate that the interface strength is sufficiently weak that interfacial cracks initiate and propagate before local stresses become high enough to cause macroscopic deformation within the epoxy. This postulate is consistent with direct measurements of the stress to shear two surfaces interacting by van der Waals interactions over a range of normal loads in the surface forces apparatus, where the measured values (1-3 MPa) are far below the yield stress of the epoxy ($\sigma_y \sim$ 50 MPa in shear) [28]. Since van der Waals forces are nonlocal and the integrated interaction does not change as the ring is rotated, at full ODTS coverage the napkin-ring test is a friction measurement. At reasonable normal loads, such an interface cannot support local stresses high enough to cause deformation in the epoxy. We conclude that regime I is characterized by brittle fracture.

Regime II. Adhesive/ductile. In regime II, the failure is also purely interfacial, as determined by TOF-SIMS analysis of the fracture surfaces using the deuterium-labeled

epoxy. However, in this regime significant macroscale deformation of the epoxy is observed, which increases with decreasing ODTS coverage. With decreasing ODTS coverage, a greater number of acidic silanol groups on the silicon oxide surface are available for strong acid-base interaction with the amine groups of the epoxy [15]. We postulate that at the beginning of regime II (contact angle 104°), the strength of the interfacial interactions becomes sufficient to support local stresses which are high enough to cause deformation within the epoxy. We define a quantity $\sigma_{I,max}$ as the maximum local stress that the interface can support, and propose $\sigma_{I,max} \approx \sigma_y$ as the criterion for the onset of deformation in the epoxy and the strong increase in fracture stress. We note that the observed deformation could occur either prior to or during unstable crack propagation. However, the former is more consistent with the sharp rise in stress in Figure 10. Deformation prior to crack propagation would lead to stress gradients, such that a large increase in applied stress would be required to achieve a small increase in the stress at the interface. Following this postulate, we will be exploring the rate and temperature dependence of the fracture stress in future work.

We note that the increase in fracture stress and the change in fracture mode (adhesive to cohesive) are not related to a wetting transition of the epoxy, as the liquid epoxy contact angle is finite and varies smoothly over the entire range of ODTS coverage where the strong increase in fracture stress occurs. This indicates that the change in fracture behavior is not related to equilibrium thermodynamics. A similar conclusion was reported recently from molecular dynamics simulations of the fracture of glassy polymer / solid interfaces in tensile [29]. These simulations indicate that local stresses govern the fracture processes rather than surface energies for such systems. As the authors point out, if the location of failure were determined by the minimum increase in interfacial free energy, the adhesive to cohesive transition would occur when the epoxy fully wets the substrate, i.e. when $S = W_{adh} - W_{coh} = 0$. This is clearly contrary to the present results.

Regime III. Cohesive. In regime III we assume that the crack initiates within the bulk epoxy because the fracture stress is independent of ODTS coverage. This is consistent with the observation that some degree of epoxy is left on the substrate surface. (However, we note that in our analysis of the fracture surfaces we were unable to identify the specific location where the crack initiated.) We find that there is a wide range of ODTS coverage for which fracture initiates within the bulk epoxy rather than on the interface. In particular, from Figure 10b we find that up to 80% of the reactive sites on the substrate surface can be occupied/blocked by ODTS without affecting the critical fracture stress. Also, from Figure 10a we find that the surface can be altered from hydrophilic (completely wet by water) to substantially hydrophobic (equilibrium water contact angle of 98°) before any decrease in the fracture stress is observed. Only a small proportion of strong acid-base interactions are required for the fracture to initiate cohesively within the epoxy. Once the interface strength is sufficient to support σ_y locally, deformation occurs in the epoxy and this likely leads to the growth of heterogeneities and cohesive crack initiation. Further increase in interface strength has no effect on the fracture stress.

To summarize, the key observation related to the transition in fracture behavior is that the strong increase in fracture stress in regime II coincides with the onset of significant deformation within the epoxy, while the fracture remains purely adhesive. In other words, the rise in the fracture stress coincides with the onset of deformation in the epoxy rather than a transition from adhesive to cohesive failure. At a critical value of interface strength, stress within some macroscopic portion of the material has apparently attained σ_y. Thus, we suggest that with increasing interface strength (or decreasing ODTS coverage), the fracture mode changes from adhesive-brittle (Regime I), to adhesive-ductile (Regime II), to cohesive (Regime III). We postulate that the adhesive–brittle to adhesive-ductile transition occurs when $\sigma_{I,max} \approx \sigma_y$. The increase in

fracture stress is likely due to stress gradients through the bond line as material deformation occurs. We suggest that the adhesive to cohesive transition then occurs due to heterogeneities that arise in the bulk epoxy during deformation.

It would be very useful to calculate $\sigma_{I,max}$ from a knowledge of the fundamental interfacial interactions, as the criterion $\sigma_{I,max} \approx \sigma_y$ could then be used to determine where a particular adhesive/substrate system (loaded in pure shear) falls with respect to the transition from adhesive-brittle to adhesive-ductile fracture. We estimate $\sigma_{I,max}$ below for the two extremes of i) a purely methylated surface, i.e. purely van der Waals interactions, and ii) no ODTS coverage which corresponds to a mixture of chemical (H-bonding) and van der Waals interactions. For purely van der Waals interactions, $\sigma_{I,max}$ should in principle approach zero in this geometry in the absence of a normal load. However, due to a finite normal force, the experiment measures a stress due to friction. As mentioned earlier, direct experimental measurements of the stress to shear two methyl terminated SAMS in the SFA yield values in the range of 1-4 MPa [23,24].

To estimate $\sigma_{I,max}$ for the bare silicon oxide/epoxy interface, we use direct measurements of the force required to separate a NH_2-terminated SAM from a COOH-terminated SAM using the interfacial force microscope [30]. After correcting for the geometry (sphere-on-plane to plane-on-plane), the measured value is 3400 +/- 316 MPa. However, $\sigma_{I,max}$ is far less than this value for at least two reasons. First, the areal density of chemical interactions between the epoxy and the silicon oxide is far lower than the areal density of chemically interacting sites in close-packed SAMS. This reduction is estimated to be roughly a factor of 10 for the present system [31]. Second, $\sigma_{I,max}$ is not simply the sum of the interfacial interactions over a unit area, because all interactions are not broken simultaneously. There is a distribution of site separation in time and in strain.

This distribution of site separation is different for SAMs and for an epoxy on silicon. The difference has been estimated to be roughly a factor of 3 for the present system from molecular dynamics simulations [32]. Therefore, we estimate $\sigma_{I,max}$ for the epoxy on bare silicon oxide to be ~ 110 MPa. This estimate is a lower bound [31]. While this is only a rough estimate, it is sufficient to show that $\sigma_{I,max} >> \sigma_y$ in the absence of ODTS. Thus, $\sigma_{I,max} << \sigma_y$ for full coverage of ODTS and $\sigma_{I,max} >> \sigma_y$ in the absence of ODTS. The fact that $\sigma_{I,max}$ crosses σ_y as a function of ODTS coverage is consistent with our postulate that the transition occurs when $\sigma_{I,max} \approx \sigma_y$. Were the value of $\sigma_{I,max}$ for epoxy on bare silicon oxide known precisely, the value of $\sigma_{I,max}$ at the transition could be estimated by multiplying by the fraction of available sites at the transition (~ 0.2 -0.3), since dispersion interactions are negligible. This could then be compared directly with σ_y. Further work is required to establish $\sigma_{I,max}$ with greater accuracy.

The relationship between the strength of interfacial interactions and the fracture stress in shear for an epoxy/substrate system has recently been examined by MD simulations. These simulations examine a small region (< 1000 Å) near the substrate on time scales which are short compared to experimental time scales. In the simulations, a model epoxy was allowed to interact with a substrate surface either through a Lennard-Jones potential or through a much stronger potential representing a chemical bond. The fraction of sites on the substrate surface able to chemically bond with the epoxy (n) was varied from 0 to 1.0. The fracture stress was found to increase linearly with n as $\sigma = 0.61 n + 0.8$, which contrasts sharply with the data in Figure 10. In the simulations, the failure was always interfacial, due to a lower areal bond density between the epoxy and the walls than within the bulk epoxy. For this reason, the plateau observed in our experimental

system was not observed in the simulations. More importantly, the rise in fracture stress in Figure 10 indicates a much stronger dependence of σ on n than was observed in the simulations. The simulation results are more indicative of brittle fracture. This supports the notion that the sharp rise in stress observed experimentally is due to large length scale deformation and stress gradients, which are not observed on the length and time scales of the simulations.

The simple picture of the transition in the above discussion becomes more complicated when the estimated local stress levels are compared with the applied stress. In particular, material deformation is observed throughout regime II despite the fact that the applied stresses are well below σ_y. Thus, stress concentration must occur within the bond line. We suggest three possible sources for stress concentration. First, whereas the silicon is very smooth, large asperities are present on the rings. For the thin bond lines in the present work, asperities from the ring surface could cause local stress concentrations at the silicon/epoxy interface. Second, slight misalignment of the rings could also lead to stress concentration. To address these two issues, samples with well-defined but variable bond thicknesses will be fabricated in future work. We note that the crosslink density within ultrathin films of the present epoxy mixture on silicon has been examined by swelling and neutron reflection [33]. The crosslink density was found to be quite uniform, except in very close proximity to the substate (~ 20 Å). Thus gradients in crosslink density do not appear to be the source of the stress concentration responsible for the observed macroscale deformation. A final possible source of stress concentration is the presence of voids or defects on the substrate surface. While there is no wetting transition of the uncured epoxy in the relevant range of ODTS coverage, flaws or voids may develop as a result of volume shrinkage and the resulting stresses which develop during cure.

Finally, the difference in the in-plane distribution of bonding sites represented in Figure 1 has no effect on the fracture curves. The fracture behavior appears to correlate with area fraction and is insensitive to the variation in lateral distribution as achieved with the two modes of deposition. This seems to suggest that the relevant length scale for the local stress is larger than the length scale of the heterogeneity of the monolayers (several microns).

Summary

Through the use of self-assembling ODTS monolayers, we have explored the relationship between the strength of interfacial interactions and the fracture stress for pure shear loading. We find a highly nonlinear relationship, with a sharp increase in fracture stress occurring over a narrow range of interface strength. The rise in the fracture stress coincides with the onset of deformation in the epoxy rather than a transition from adhesive-to-cohesive failure, although the latter transition follows closely after the onset of deformation in the epoxy. We postulate that an adhesive–brittle to adhesive-ductile transition occurs when the interface can support local stresses which are comparable to σ_y. This is consistent with estimates of the maximum stresses that can be supported by interfaces of epoxy with fully methylated or bare silicon oxide surfaces. These estimates indicate that the interface strength crosses σ_y at some partial coverage of.ODTS. The low value of interface strength for full ODTS coverage is a result of the fact that van der Waals interactions contribute negligibly in shear for a smooth, planar surface. By contrast, in tensile loading van der Waals interactions result in a large interfacial strength such that for those interactions alone the interface strength likely exceeds σ_y of most polymeric adhesives. Thus, we would not expect the adhesive-brittle to adhesive-ductile

transition observed here to occur for tensile loading. Surprisingly, the fracture behavior is insensitive to the variation in in-plane distribution of ODTS achieved with island or homogeneous growth modes of deposition.

ACKNOWLEDGMENTS

Sandia is a multiprogram laboratory operated by Sandia Corporation, a Lockheed Martin Company, for the United States Department of Energy under contract DE-AC04-94AL85000.

REFERENCES

1. Pocius, A. V., *Adhesion and Adhesives Technology*, (Hanser, Cincinnati, OH, 1997).
2. Lee, L .H. Ed., *Fundamentals of Adhesion* (Plenum Press, New York, NY,1991).
3. Wu, S., *Polymer Interface and Adhesion* (Marcel Dekker, New York, NY, 1982).
4. Kinloch, A. J., Young, R. J., *Fracture Behavior of Polymers* (Elsevier Applied Science, New York, NY, 1983)
5. Cave, N. G., Kinloch, A. J. *POLYMER*, **33**, 1162, (1992).
6. Zhuk, A. V., Evans, A. G., Hutchinson, J. W., Whitesides, G. M. *J. Mater. Res.* **13**, 3555, (1998).
7. Mittal, K. L., in *Adhesion Science and Technology*, Lee, L. H., Ed., (Plenum Press, New York, NY, 1975).
8. Gent, A. N., Schultz, J. *J. Adhesion*, **3**, 281, (1972).
9. Andrews, E. H., Kinloch, A. J. *Proc. Roy. Soc. Lond. A.*, 332, 385, (1973); Andrews, E. H., Kinloch, A. J. *Proc. Roy. Soc. Lond. A.*, 332, 401, (1973).
10. Kim, S., Choi, G. Y., Ulman, A., Fleischer, C. *Langmuir* **13**, 6850, (1997).
11. Brown, H. R. *Macromolecules* **24**, 2752, (1991).
12. Creton, C., Kramer, E. *Macromolecules* **25**, 3075, (1992).
13. Washiyama, J., Kramer, E. J., Hui, C. Y. *Macromolecules* **26**, 2928, (1993).
14. Washiyama, J., Kramer, E. J., Creton, C. F., Hui, C. Y. *Macromolecules* **27**, 2019, (1994).
15. Gutowski, W. in *Fundamentals of Adhesion*, Lee, L .H. Ed., (Plenum Press, New York, NY,1991).
16. Wasserman, S. R., Whitesides, G. M., Tidswell, I. M., Ocko, B. M., Pershan, P. S., Axe, J. D. *J. Am. Chem. Soc.* **111**, 5852, (1989).
17. Carraro, C., Yauw, O., Sung, M. M., Maboudian, R. *J. Phys. Chem. B*, **102**, 4441, (1998).

18. Bierbaum, K., Grunze, M., Baski, A. A., Chi, L. F., Schrepp, W., and Fuchs, H. *Langmuir*, **11**, 2143, (1995).

19. Banga, R., Yarwood, J., Morgan, A. M., Evans, B., and Kells, J. *Langmuir*, **11**, 4393, (1995).

20. Kent, M. S., McNamara, W. F., Baca, P. M., Wright, W., Domeier, L. A., Wong, A. P. Y., Wu, W. L *J. Adhesion* **69**, 139, (1999).

21. Russell, T. P. *Mater. Sci. Rep.*, **5**, 171, (1990).

22. Adams, R. D., Wake, W. C. *Structural Adhesive Joints In Engineering*, (Elsevier Applied Science, New York, NY, 1984).

23. Adamson, A. W., Gast, A. P. *Physical Chemistry of Surfaces*, (John Wiley & Sons, New York, NY, 1997).

24. Allara, D., Parikh, A. N., Judge, E. *J. Chem. Phys.* **100**, 1761, (1994).

25. Yamada, S., Israelachvili, J., *J. Phys. Chem. B*, **102**, 234, (1998).

26. Yoshizawa, H., McGuiggan, P., Israelachvili, J. *Science* **259**, 1305, (1993).

27. The deuterated epoxy film used to calibrate the SIMS data was spin-coated onto a silicon wafer, and the thickness was measured by X-ray reflectivity. The thickness was measured prior to and after evacuation (10^{-9} torr) for 16 hours. No loss of mass upon evacuation was detected.

1. The yield stress in shear ($\sigma_{y,\,shear}$) was estimated from the measured $\sigma_{y,\,comp.}$ by:

$\sigma_{y,\,shear} = (8/9)\,\sigma_{y,\,comp.}/\sqrt{3}$. The factor of $\sqrt{3}$ comes from assuming a von Mises yield surface, and relates a uniaxial yield strength to a shear yield strength. The factor of (8/9) reflects the reduction in yield when there is no pressure.

29. Gersappe, D. Robbins, M. O. *Europhys. Lett.*, **48**, 150, (1999).

30. Thomas, R. C., Houston, J. E., Crooks, R. M., Kim, T., Michalske, T. A. *J. Amer. Chem. Soc.*, 117, 3830, (1995).

1. To estimate the interfacial bond density for the epoxy on silicon, we take the thickness (t) of the surface atomic layer to be 4 Å, and the density (ρ) to be 1.13 g/cc. An assumption must then be made regarding the composition at the interface. We assume the interfacial composition to be equal to the bulk composition. This leads to a lower limit for the interfacial bond density between epoxy and silicon. The area per T403 molecule is given by $M/(N_A \rho t)$, where M is the molecular weight of one T403 molecule plus the molecular weight of three epoxide oligomers (corresponding to a composition of 46 phr). This gives an area per T403 molecule of 523 $Å^2$. For close-packed SAMs, the area per molecule is in the range 20-25$Å^2$. Taking the larger number, the ratio of the areas per molecule for the epoxy and SAM cases is 21. There is uncertainty regarding the number of bonds between the crosslinker and the substrate surface, as there are six reactive protons but it seems unlikely for geometrical reasons that all would react. For this estimate we assume two bonds to the substrate per T403 molecule. This is an assumption that needs to be examined experimentally. With this assumption, the ratio of the number of bonds/area for the SAM and epoxy is 10.5. This value is believed to be an upper limit. Preferential segregation of the crosslinker to the interface would result in a lower factor. A lower factor will also result if the average number of bonds to the substrate per T403 molecule in the surface layer is greater than two.

32. Stevens, M. J., submitted to Macromolecules

33. H. Yim, M. Kent, W. F. McNamara, R. Ivkov, S. Satija, J. Majewski *Macromolecules* **32**, 7932, (1999).

FIGURE CAPTIONS

1. Representative AFM images of ODTS-coated silicon wafers where the ODTS deposition was performed at a) 24 °C, and b) 10 °C. Island growth occurred for all depositions at 10 °C. Only homogenous growth was observed for depositions at 24 °C.

2. Variation in ODTS coverage with exposure time of the silicon substrates to the treating solution. ODTS coverage is indicated indirectly through the equilibrium water contact angle.

3. Advancing and receding water contact angles as a function of ODTS coverage for depositions performed at a) 24 °C, and b) 10 °C. Little difference is seen in the behavior of the water contact angles for island and homogenous deposition modes.

4. Advancing and receding epoxy contact angles as a function of ODTS coverage for depositions performed at 24 °C. The epoxy is nonwetting and the contact angles vary smoothly with ODTS coverage over this range.

5. Area fraction of methyl groups versus ODTS coverage. The area fraction of methyl groups was determined using the Cassie equation and water (•) and epoxy (□) contact angle data.

6. X-ray reflectivity data used to determine mass coverage and thickness of ODTS layers for a range of ODTS coverages corresponding to the following equilibrium water contact angles: bare silicon wafer(+), 85° (x), 95.5° (□), 106° (filled triangles), 115° (•).

7. Fractional mass coverage of ODTS as determined by X-ray reflectivity versus equilibrium water contact angle for depositions performed at 24 °C (•) and 10 °C (□). The equilibrium water contact angle is not sensitive to the variation in in-plane distribution as obtained with the two deposition modes.

8. ODTS layer thickness as determined by X-ray reflectivity versus equilibrium water contact angle for depositions performed at 24 °C (•) and 10 °C (□). The layer thickness is independent of ODTS coverage for island growth mode, but decreases with decreasing coverage with homogeneous growth mode.

9. Maximum shear stress recorded in the napkin-ring test for epoxy on bare silicon using rings differing in diameter by a factor of 2. The fracture stress is independent of the diameter of the ring.

10. a) Fracture stress as a function of ODTS coverage (indicated by equilibrium water contact angle) for ODTS depositions performed at 24 °C (•) and 10 °C (□). b) Fracture stress as a function of fractional mass coverage of ODTS determined by X-ray reflectivity for ODTS depositions performed at 24 °C (•) and 10 °C (□). c) Fracture stress as a function of area fraction of methyl groups as determined from the Cassie equation for ODTS depositions performed at 24 °C (•) and 10 °C (□). d) Fracture stress as a function of the work of adhesion for the uncured epoxy on the ODTS coated substrates.

11. Normalized intensity of D^- ions from SIMS analysis of the silicon substrate after fracture as a function of the ODTS coverage. A deuterated epoxy was used in order

to distinguish epoxy resin from adventicious hydrocarbon. The signal was calibrated using a 30 Å film of deuterated epoxy. The D^- signal corresponds to a very small fraction of a monolayer, indicating that the fracture is adhesive over this range of ODTS coverage.

12. Optical micrographs showing the extent of deformation within the epoxy on the rings after fracture for the follwing range of ODTS coverage: a) equilibrium water contact angle = 113°, fracture stress < 3 MPa, b) equilibrium water contact angle = 99°, fracture stress = 13 MPa, and c) equilibrium water contact angle = 98°, fracture stress = 25 MPa.

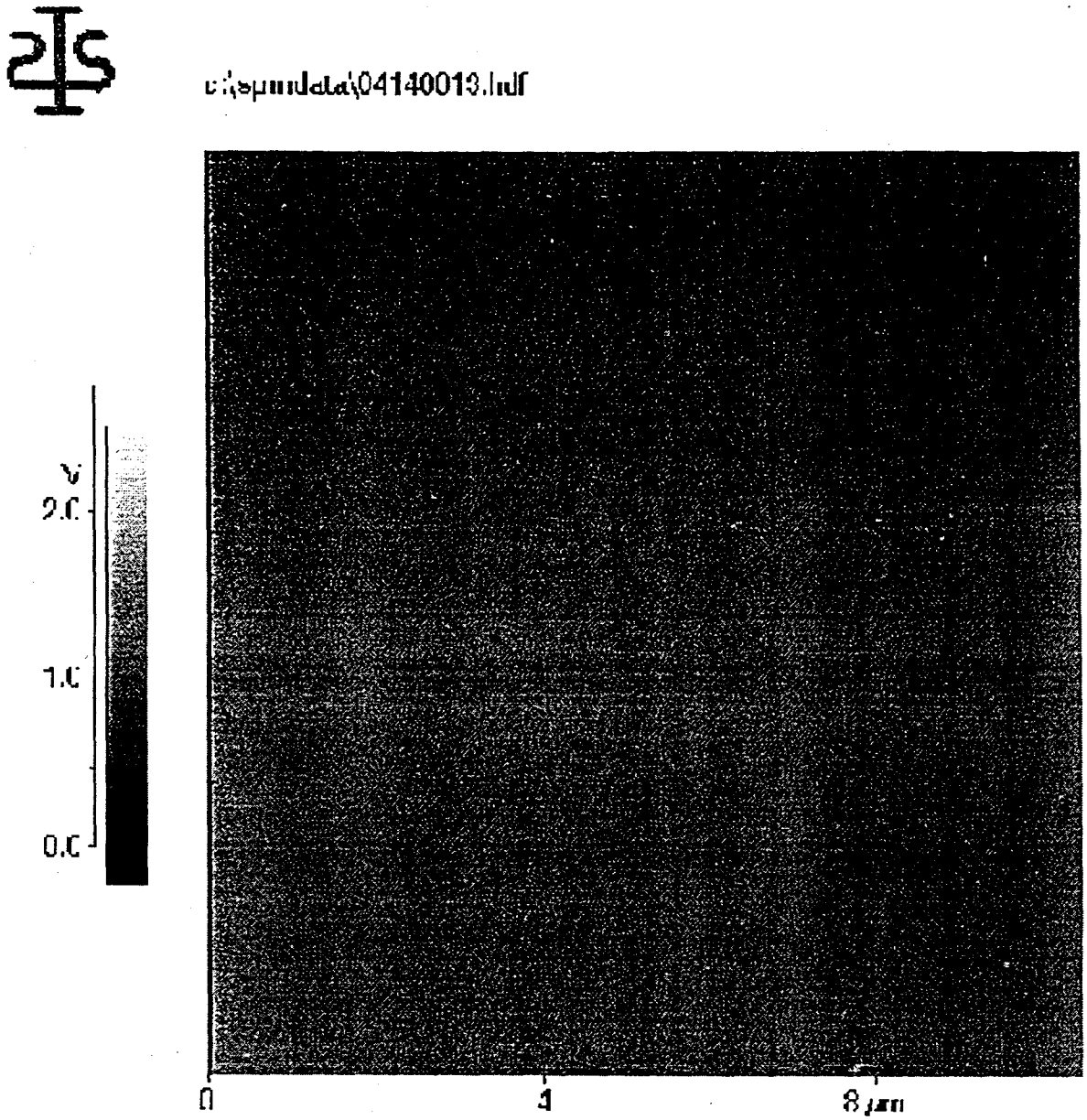
c:\spmdata\04140013.hdf
V
2.0
1.0
0.0
0
4
8 μm

c:\spmdata\04260034.hdf

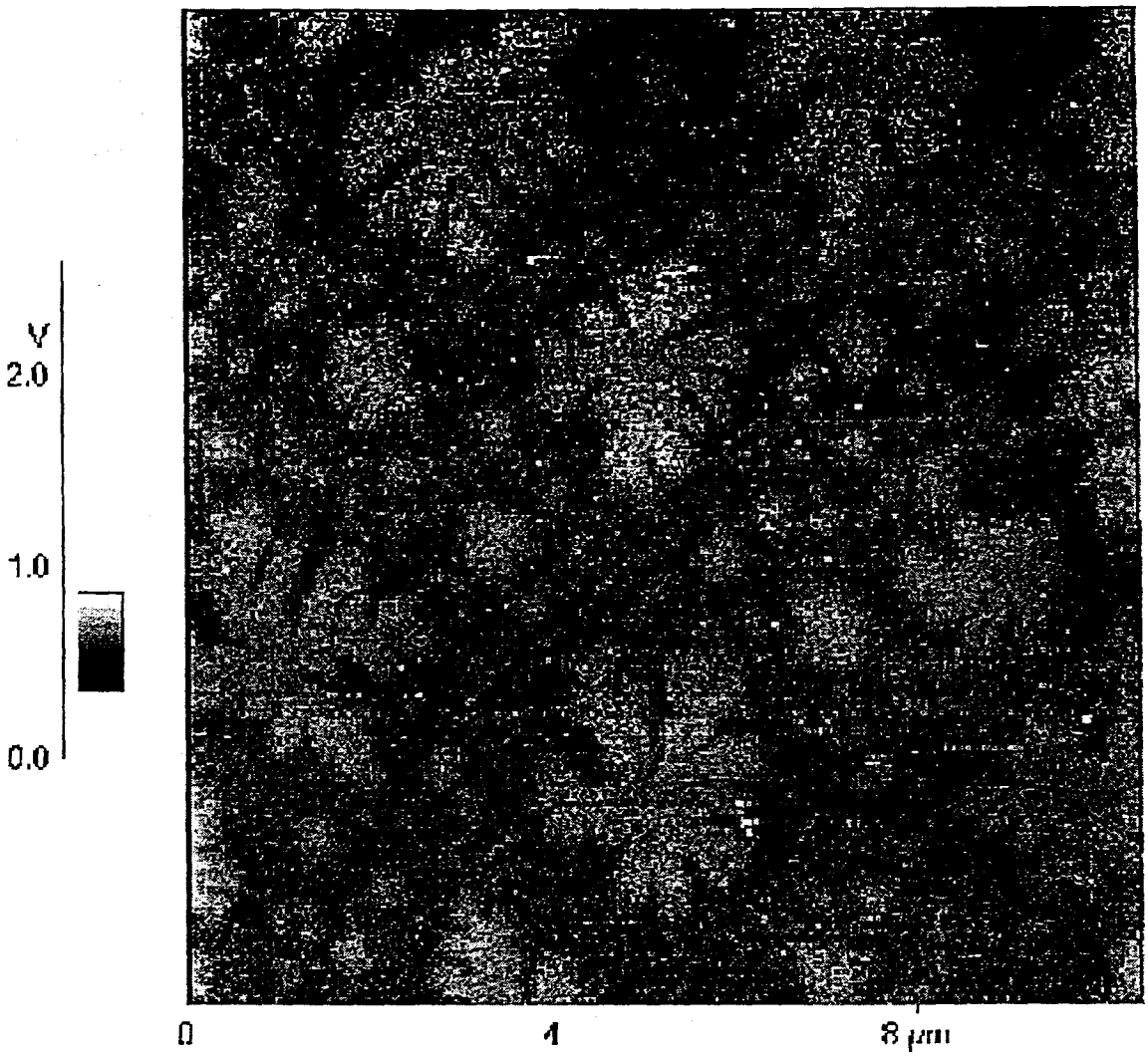

1b

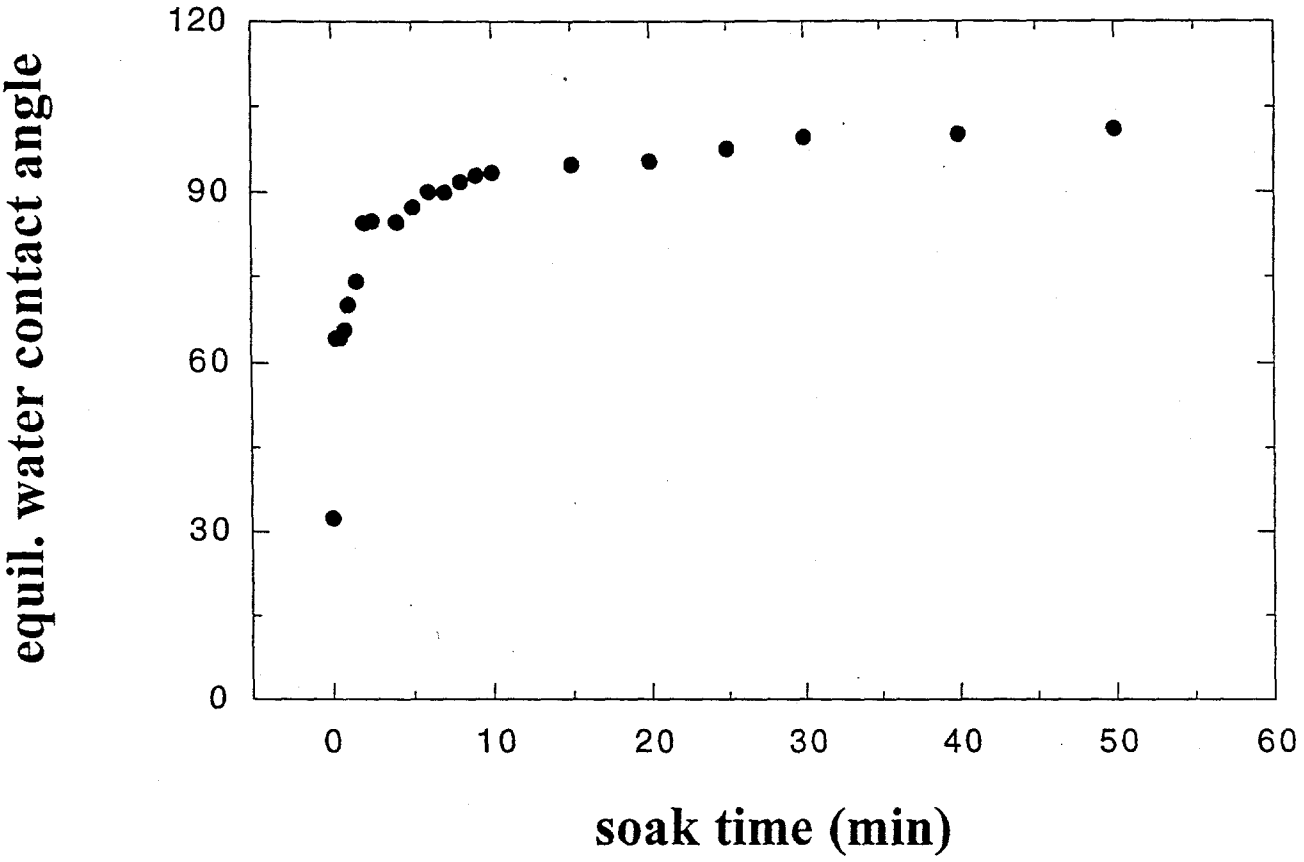
equil. water contact angle
120
90
60
30
0
0
10
20
30
40
50
60
soak time (min)

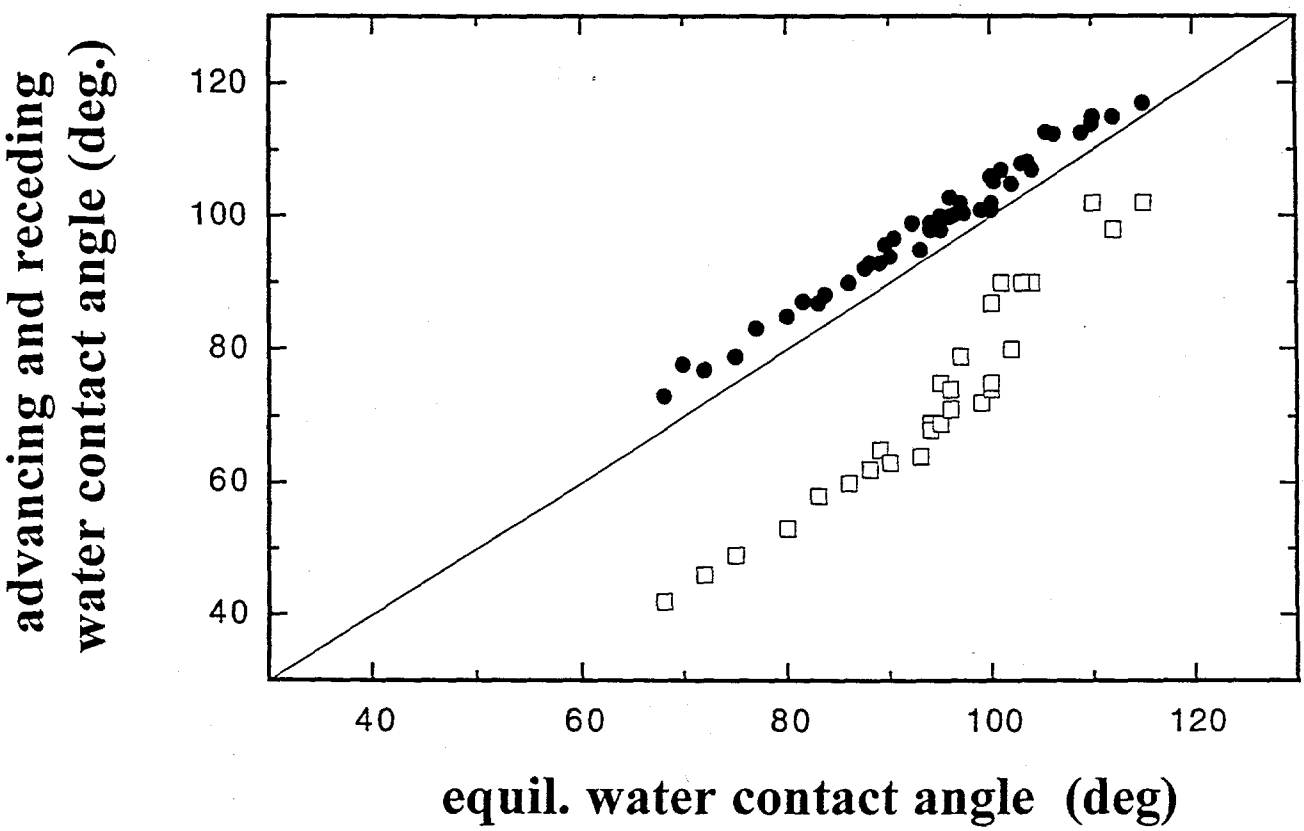
advancing and receding
water contact angle (deg.)
120
100
80
60
40
40
60
80
100
120
equil. water contact angle (deg)

3a

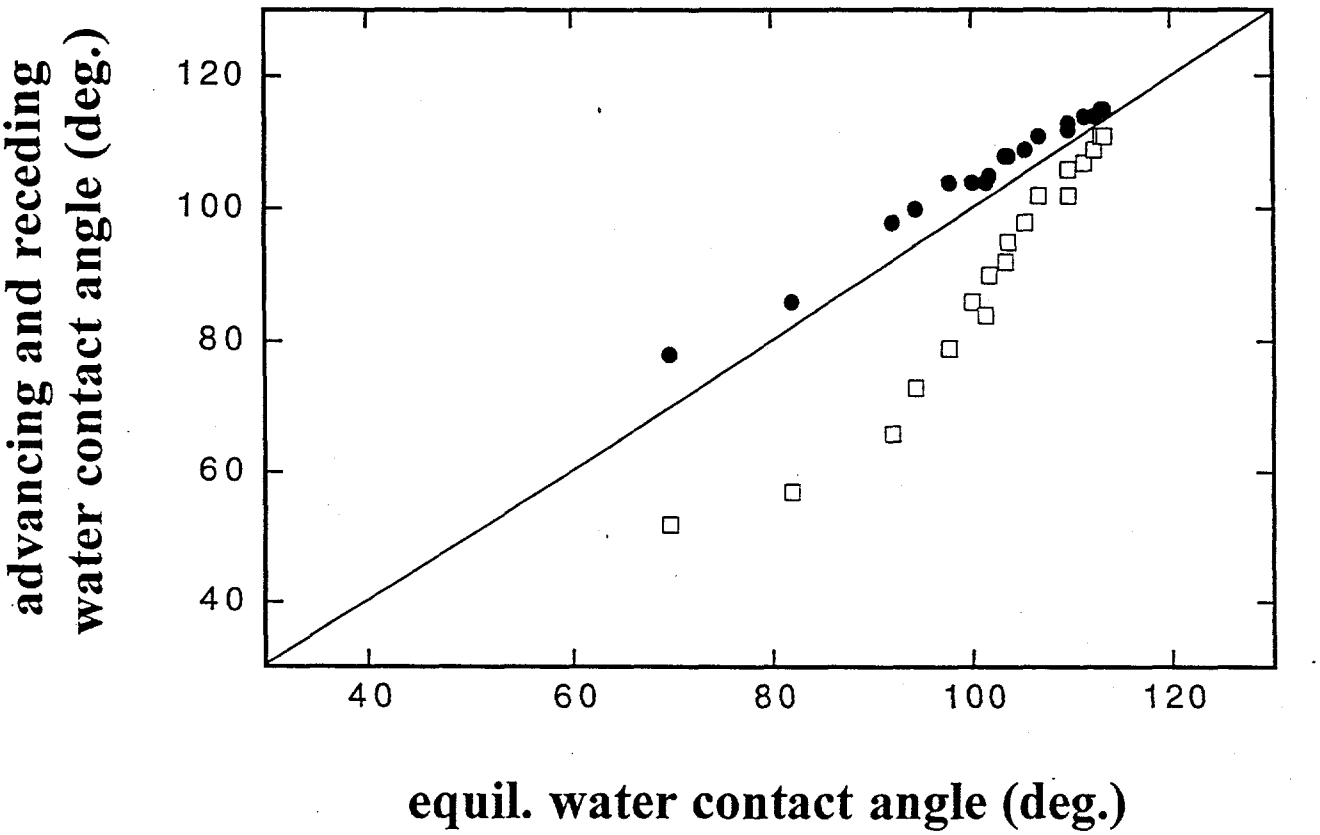
advancing and receding water contact angle (deg.)
120
100
80
60
40
40
60
80
100
120
equil. water contact angle (deg.)

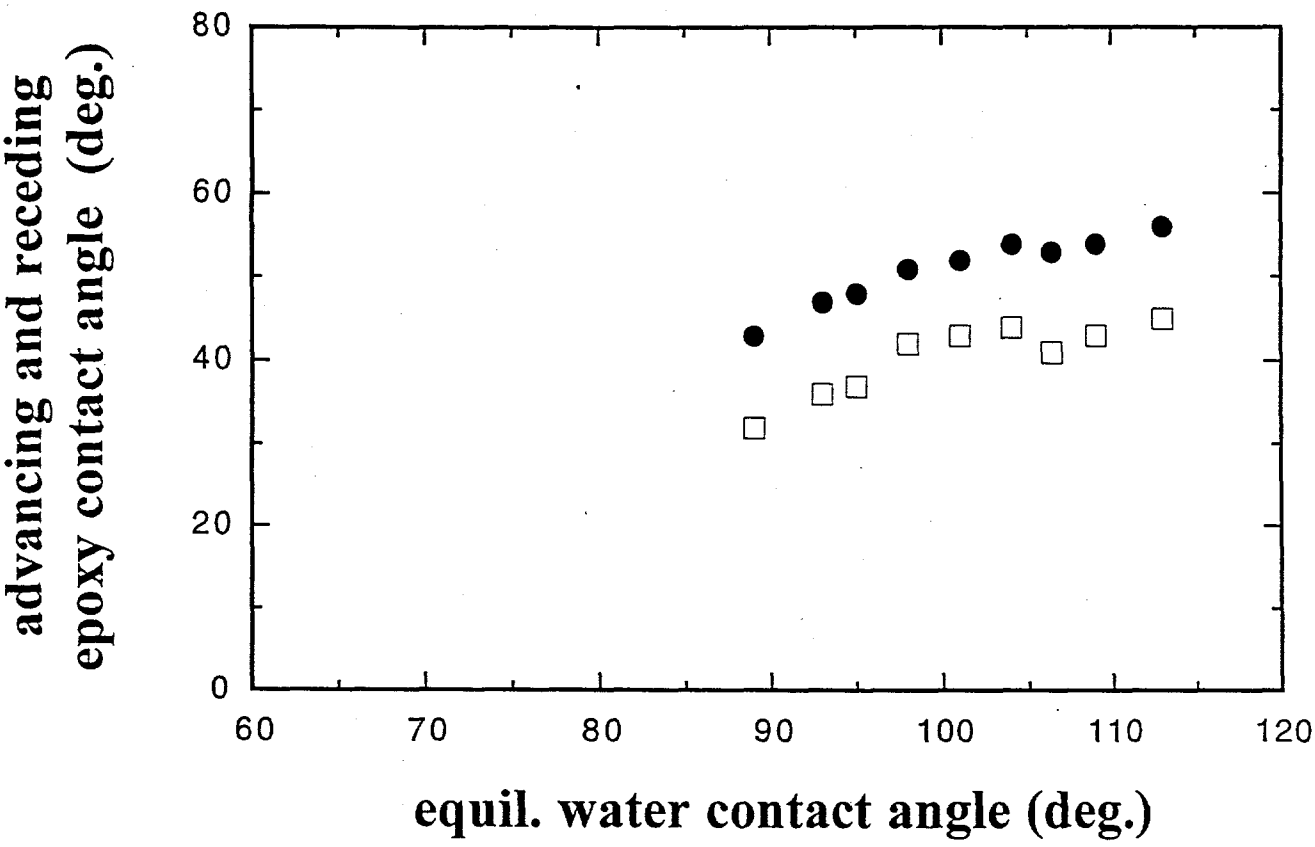
advancing and receding
epoxy contact angle (deg.)
80
60
40
20
0
60
70
80
90
100
110
120
equil. water contact angle (deg.)

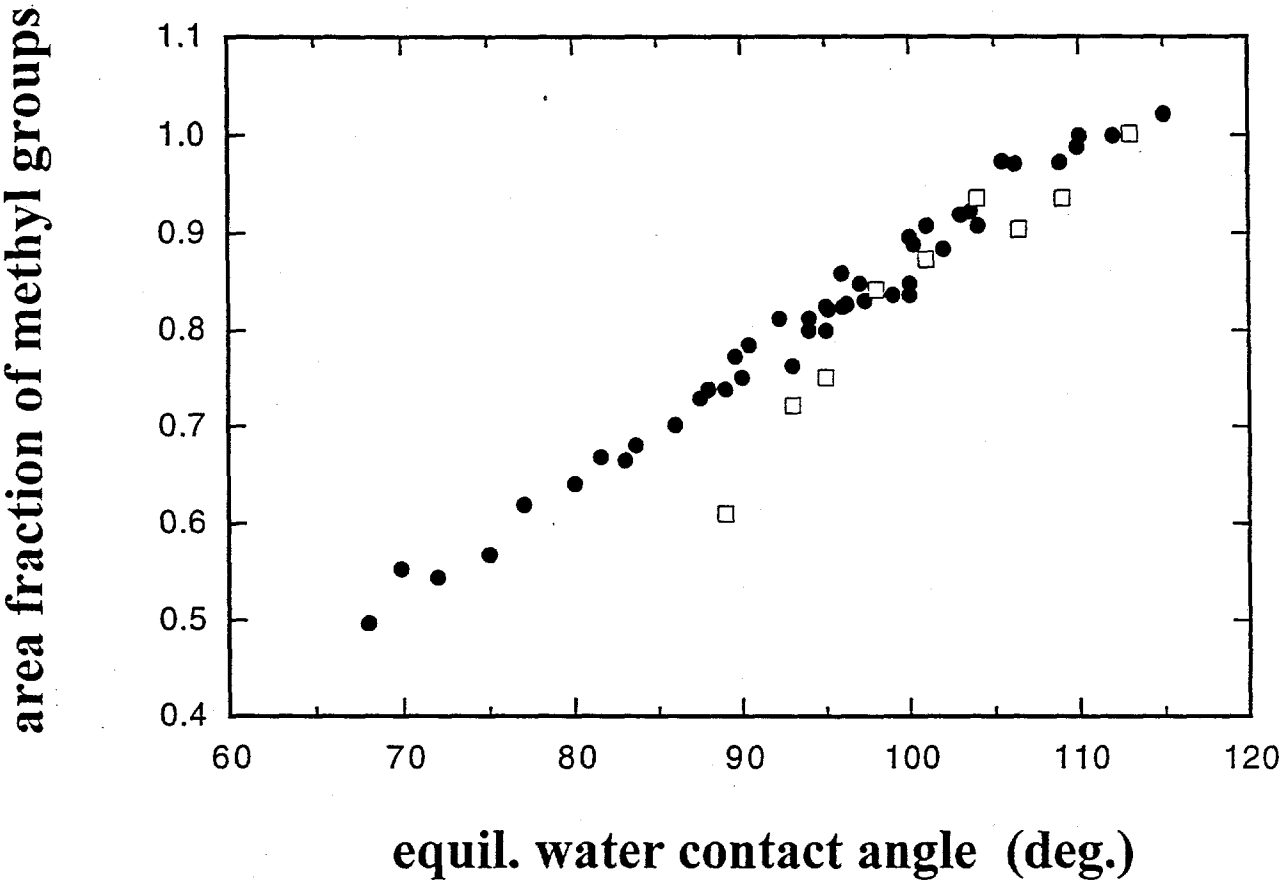
area fraction of methyl groups
1.1
1.0
0.9
0.8
0.7
0.6
0.5
0.4
60
70
80
90
100
110
120
equil. water contact angle (deg.)

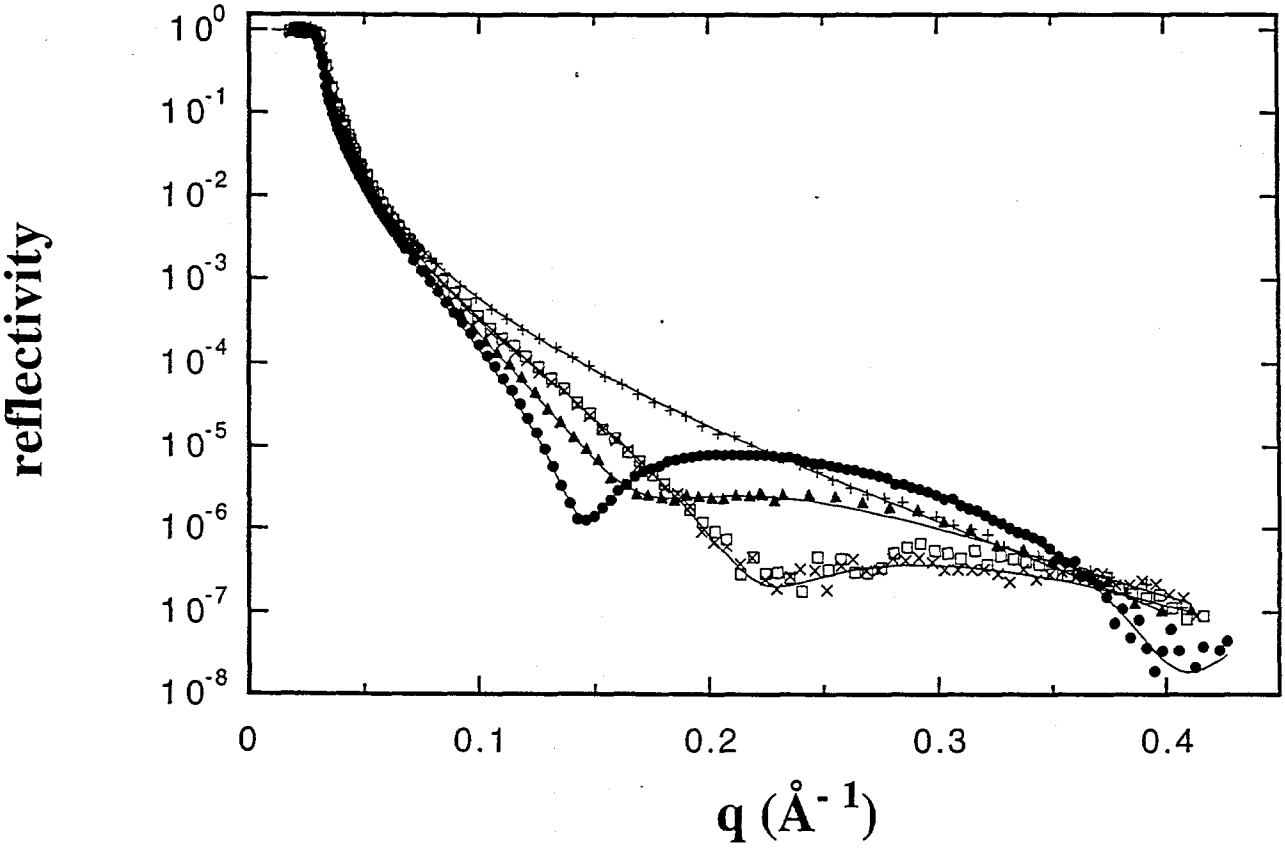
reflectivity
10^0
10^-1
10^-2
10^-3
10^-4
10^-5
10^-6
10^-7
10^-8
0
0.1
0.2
0.3
0.4
q (Å^-1)

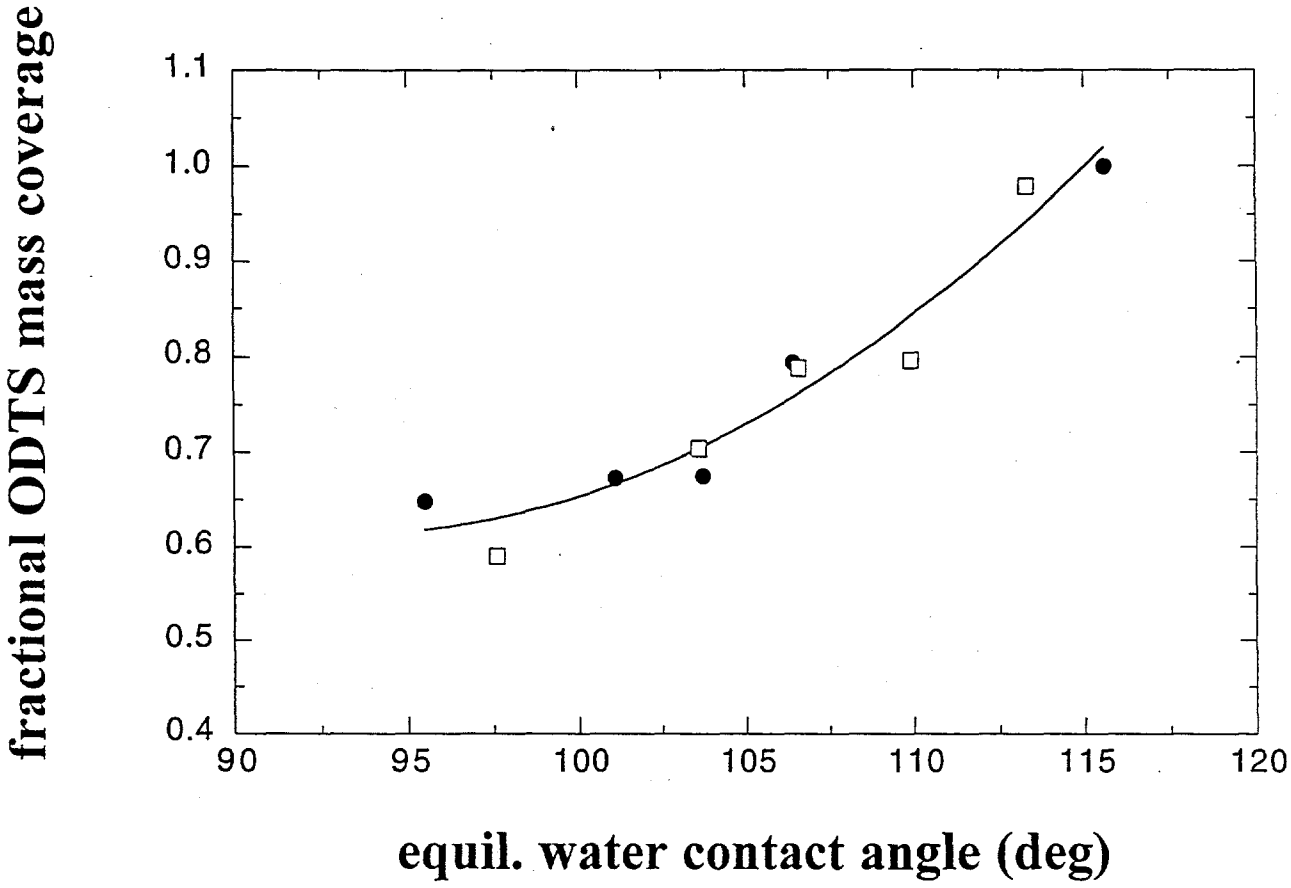
fractional ODTS mass coverage
1.1
1.0
0.9
0.8
0.7
0.6
0.5
0.4
90
95
100
105
110
115
120
equil. water contact angle (deg)

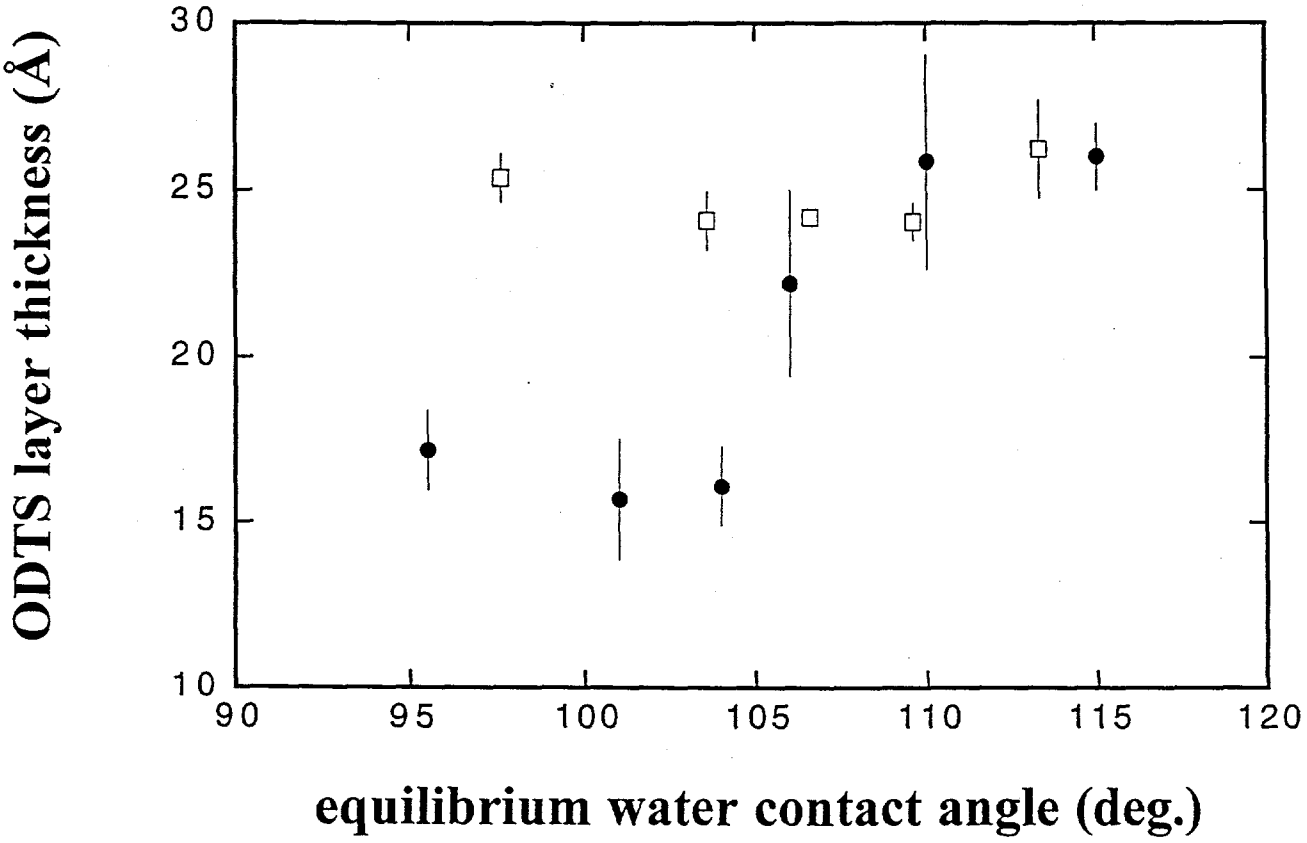
ODTS layer thickness (Å)
30
25
20
15
10
90
95
100
105
110
115
120
equilibrium water contact angle (deg.)

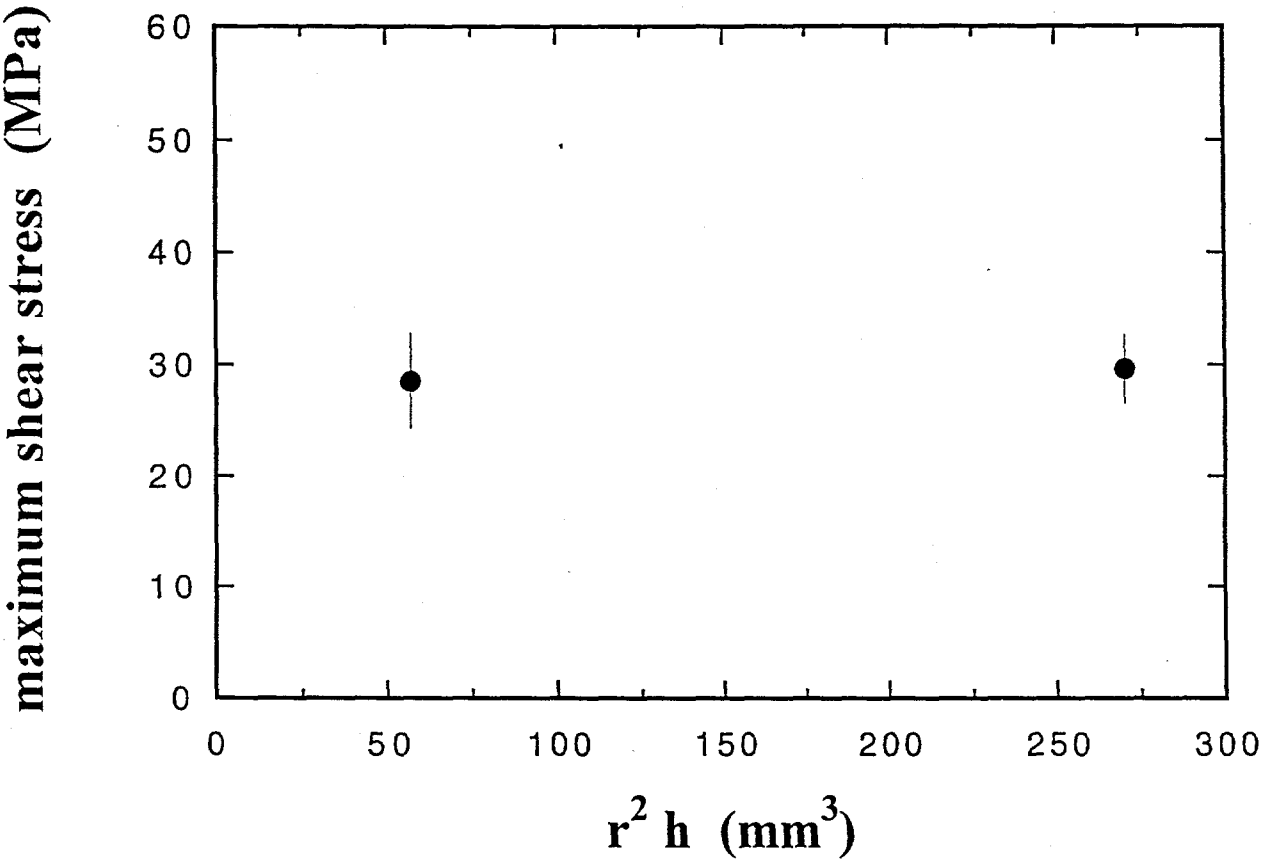
maximum shear stress (MPa)
60
50
40
30
20
10
0
0
50
100
150
200
250
300
r2 h (mm3)

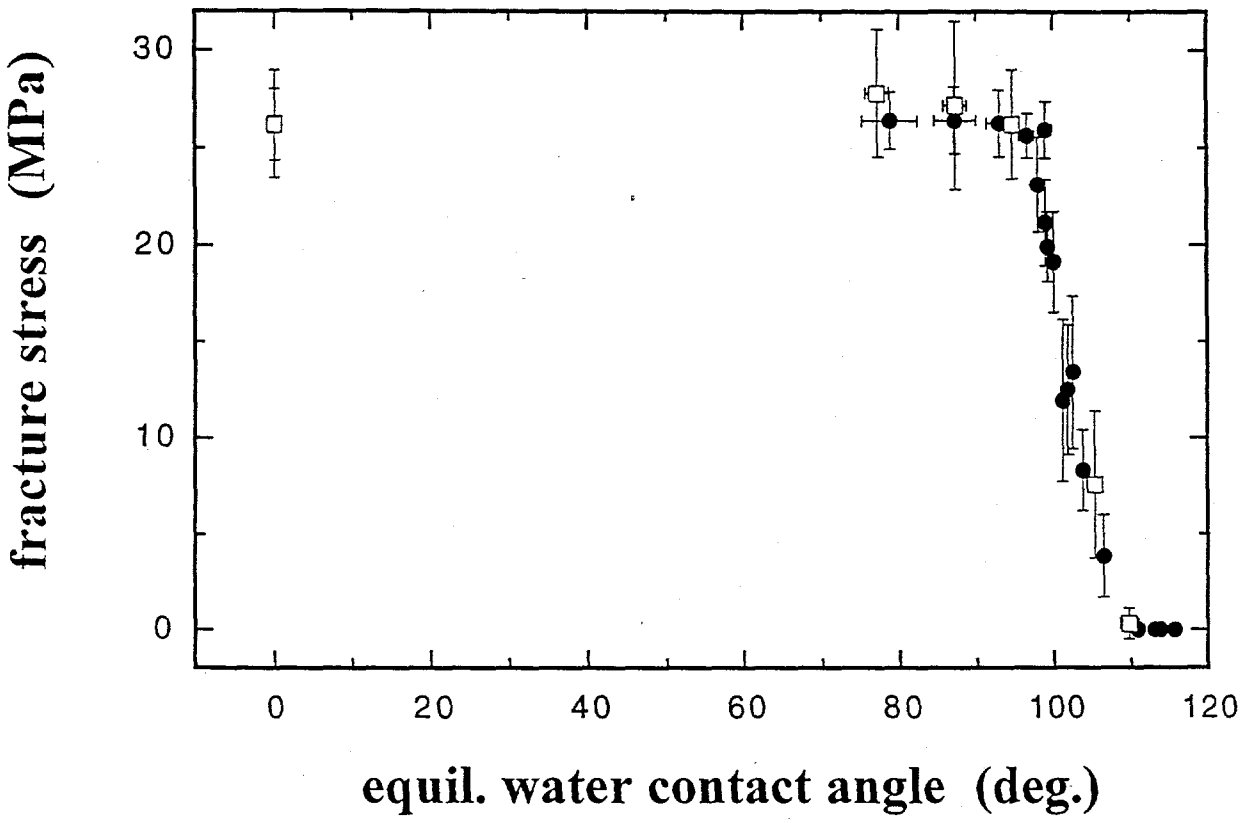
fracture stress (MPa)
30
20
10
0
0
20
40
60
80
100
120
equil. water contact angle (deg.)

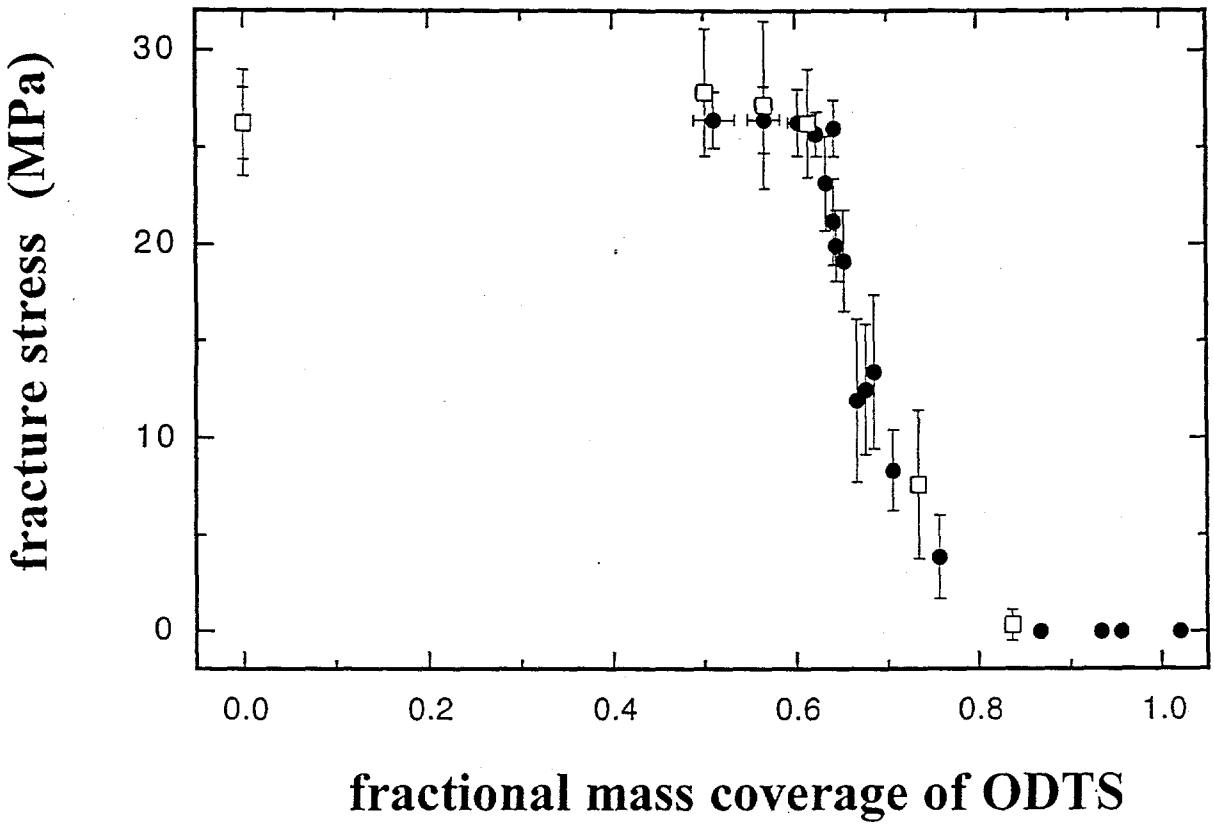
fracture stress (MPa)
30
20
10
0
0.0
0.2
0.4
0.6
0.8
1.0
fractional mass coverage of ODTS

10b

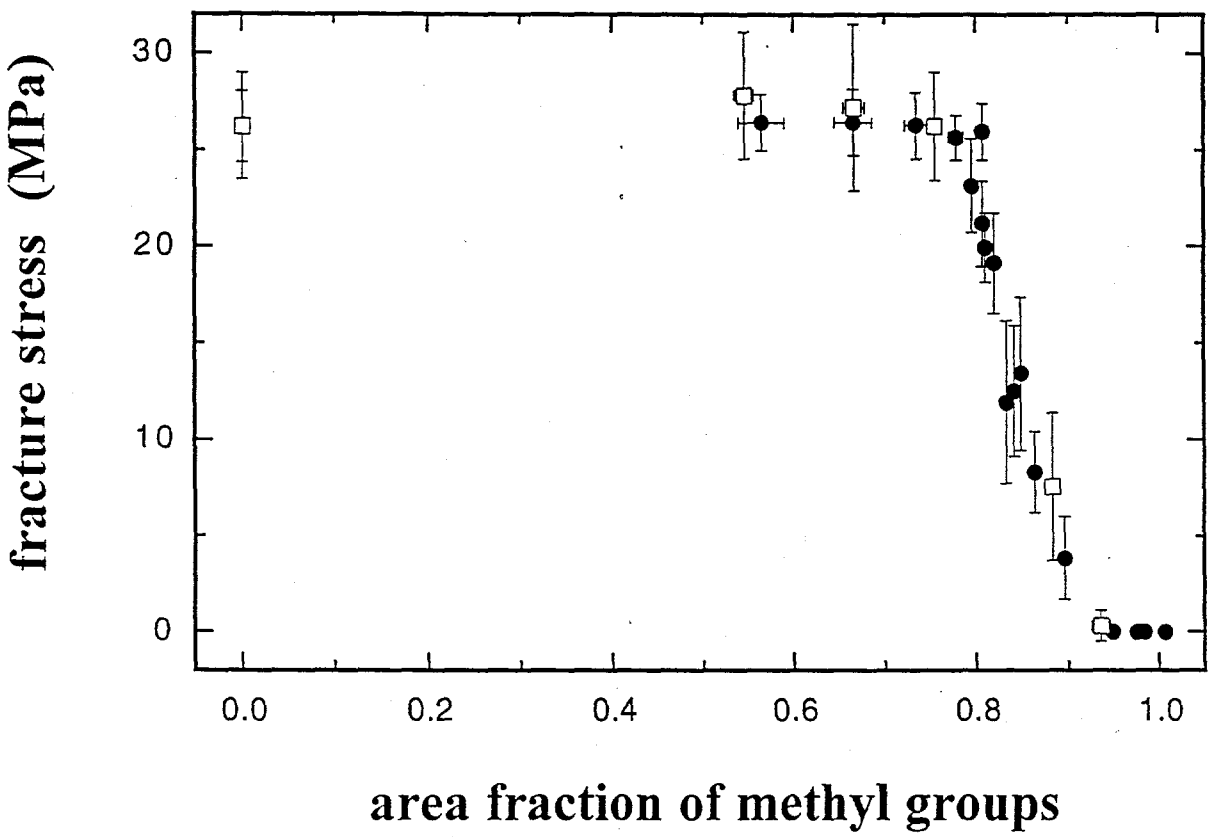
fracture stress (MPa)
30
20
10
0
0.0
0.2
0.4
0.6
0.8
1.0
area fraction of methyl groups

10c

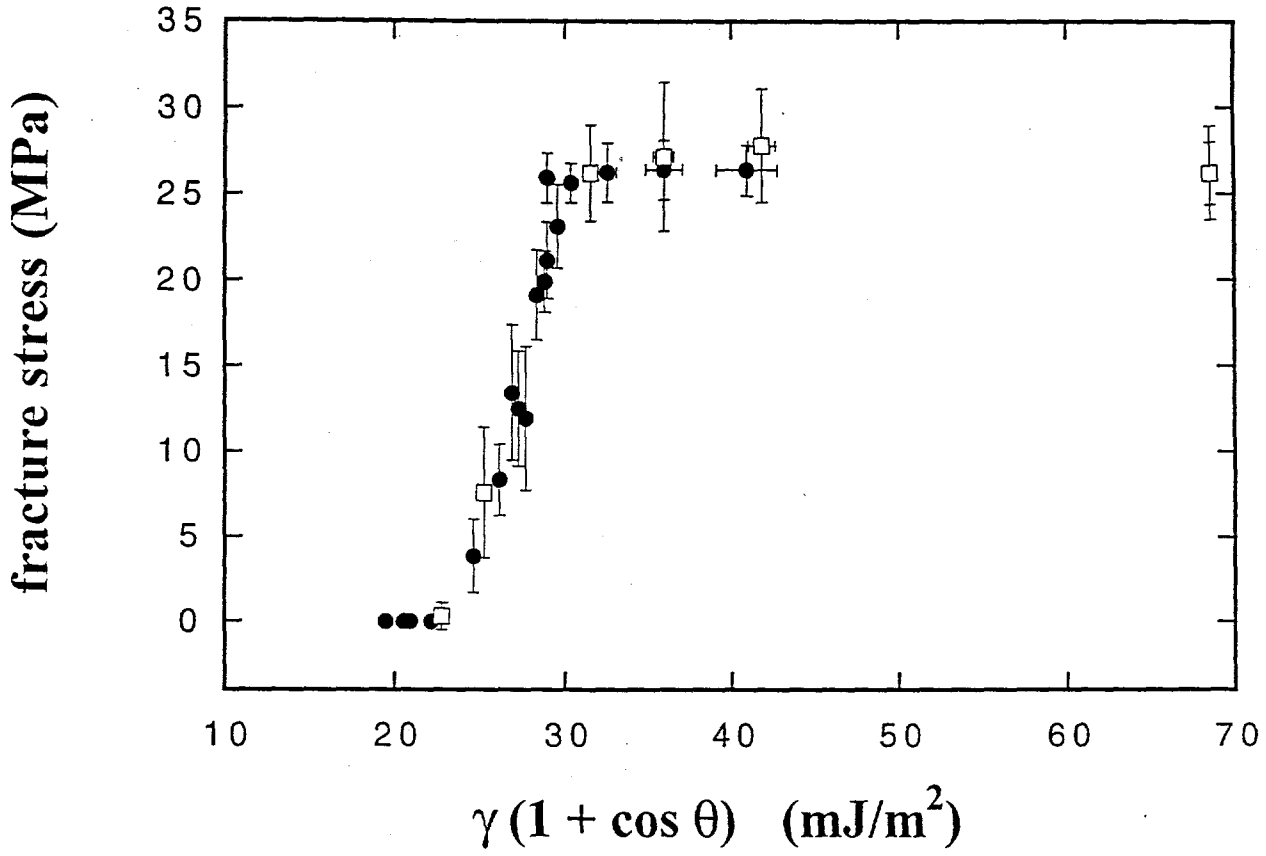
fracture stress (MPa)
35
30
25
20
15
10
5
0
10
20
30
40
50
60
70
γ (1 + cos θ) (mJ/m²)

10d

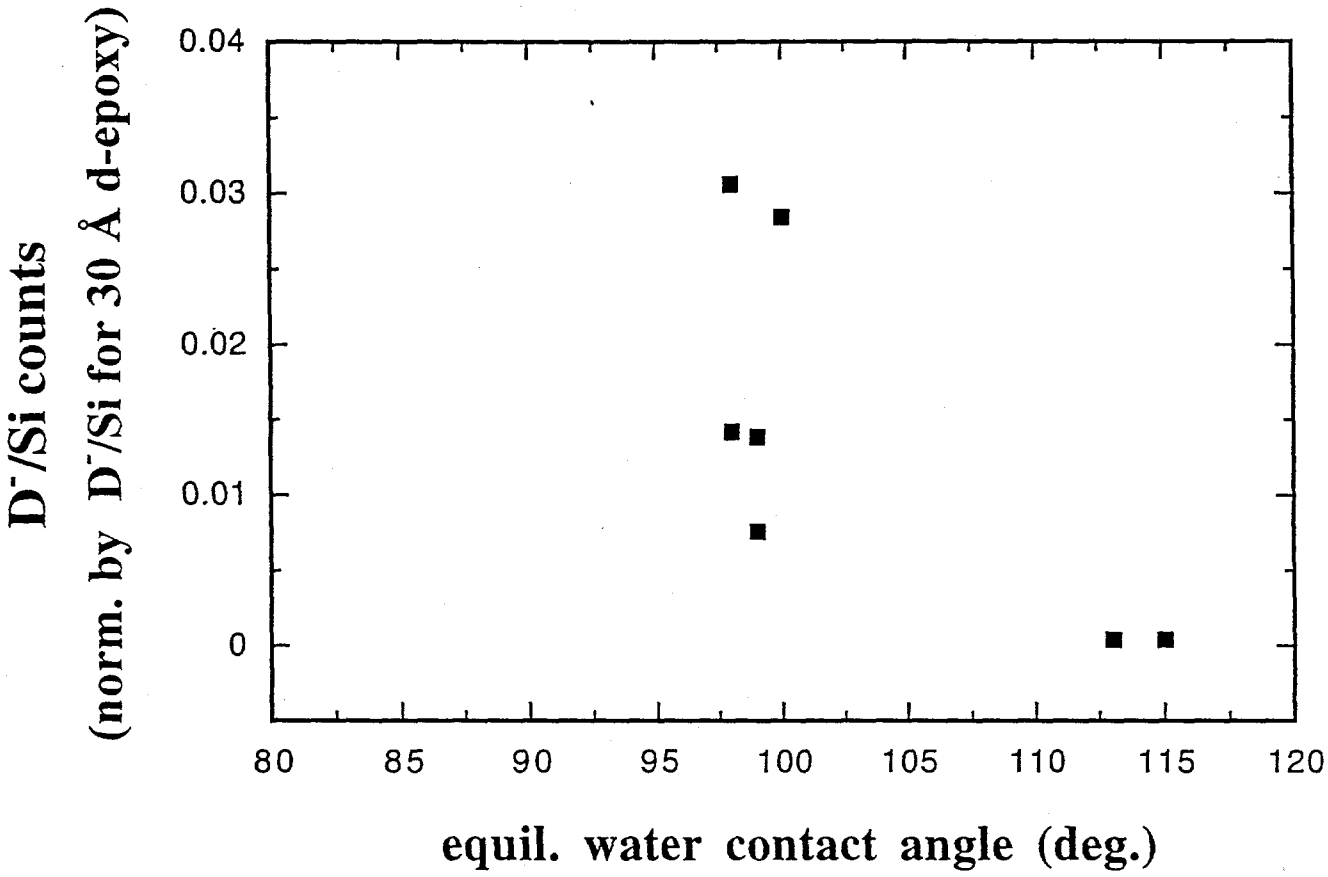
D⁻/Si counts
(norm. by D⁻/Si for 30 Å d-epoxy)
0.04
0.03
0.02
0.01
0
80
85
90
95
100
105
110
115
120
equil. water contact angle (deg.)

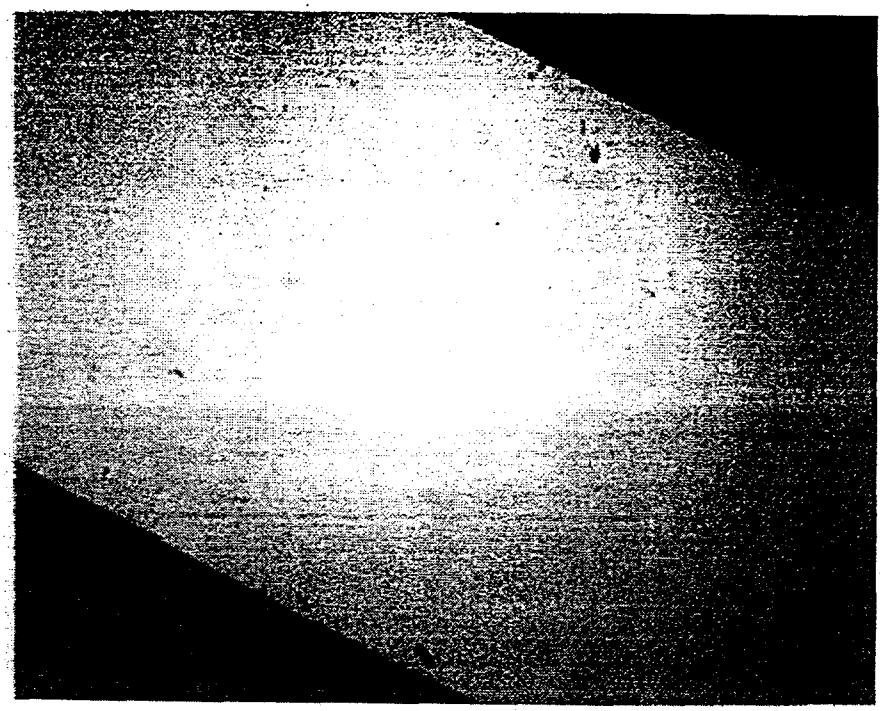

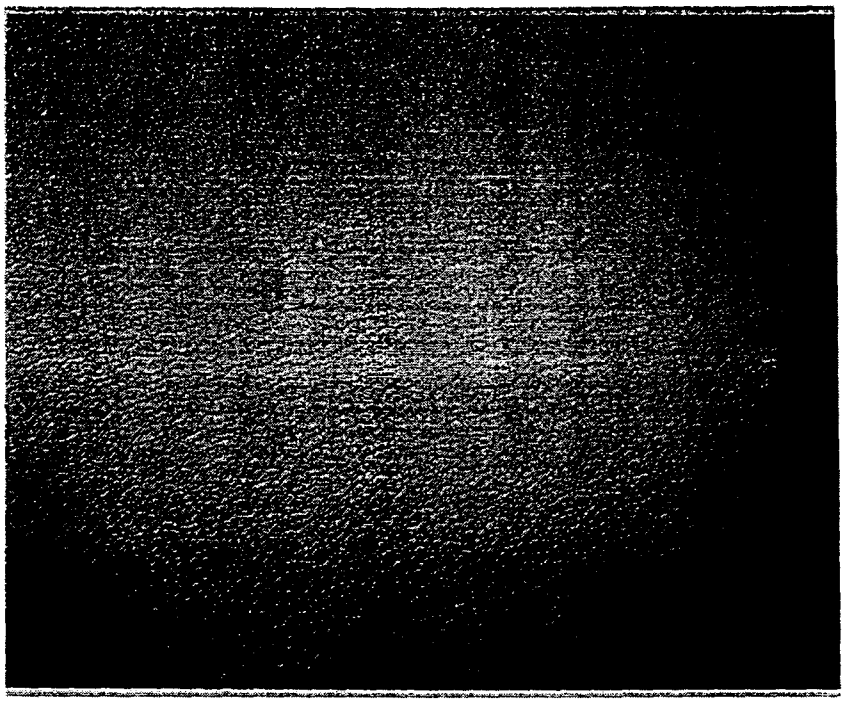

12c